Production of diamondlike carbon films through random compact cluster stacking

V. Paillard, P. Mélinon, V. Dupuis, A. Perez, J. P. Perez, G. Guiraud, and J. Fornazero
Département de Physique des Matériaux, Université Claude Bernard Lyon I, F-69622 Villeurbanne, France

G. Panczer
Laboratoire de Minéralogie et de Cristallographie, Université Claude Bernard Lyon I, F-69622 Villeurbanne, France
(Received 15 November 1993)

Carbon thin films exhibiting a different structure have been obtained using low-energy neutral-cluster beam deposition. The first-order Raman scattering of such materials exhibits some characteristic features related to the phonon density of states of diamond. A careful analysis shows that the electronic structure is not explained by a classical random network model such as Polk's model and an alternative film structure is proposed. In addition, the correlation between the free-cluster properties and the film properties seems to confirm the existence of the fullerenes in the 20–32-atom size range.

I. INTRODUCTION

Potential applications of amorphous diamondlike carbon (DLC) films greatly interest the research and industrial communities.[1] Thin films are commonly produced by several techniques such as chemical-vapor deposition (CVD), rf sputtering, low-energy carbon-ion beam, etc. Film quality and uniformity are well controlled for technological applications, but the understanding of the synthesis mechanisms, electronic structure, and properties of these materials lags behind the technology. We use a technique called low-energy neutral-cluster beam deposition (LECBD) for the elaboration of disordered tetrahedrally bonded carbon thin films. The deposition rate obtained with this technique is low compared to the usual methods, but it allows a better understanding of the film growth mechanisms.[2] From the correlation between the electronic properties of the incident free clusters and the properties of the films obtained by cluster deposition, it is possible to understand the carbon nucleation mechanisms. In addition, a memory of the specific properties of the incident clusters allows the formation of material which exhibits random compact cluster stacking (RCCS).

II. EXPERIMENTAL PROCEDURE

The laser vaporization source as described by Smalley[3] seems to be the better compromise for carbon cluster synthesis. Their formation is described in detail elsewhere.[4] Roughly, ions and neutral atoms are stripped by target rod bombardment with photons [Nd-YAG (yttrium aluminum garnet) laser-pulsed source] inside a vacuum cavity. The different species create a hot plasma (about 10^4 K) that is strongly thermalized by high-pressure cold helium gas, injected in the cavity by a pulsed valve. The laser shots take place during the peak carrier gas flow. The cold gas-plasma mixture induces a nonequilibrium state so that a cluster embryo can grow after each pulse. These species are then rapidly quenched during the following isentropic expansion into the vacuum. To increase the size range of clusters, the mean residence time of the plasma-gas mixture is increased. The geometry of our cluster source is similar to the Milani and deHeer source.[5] Cluster mass distributions are analyzed in a time-of-flight mass spectrometer. Either natural ions or photoionized neutral clusters using a frequency-doubled dye laser pumped by a XeCl excimer laser can be used for this purpose. Before acceleration, the kinetic energy of the free clusters is about 10–20 eV. To avoid any charge effect on the substrates (sapphire, Corning glass, silicon) during deposition, the ions are deflected in front of the sample holder so that only neutral clusters are deposited. The pressure is about 10^{-4} Pa in the chamber during the film growth. *In situ* electrical properties are performed by conductance measurements of the films. The typical thin-film thickness, measured by a crystal quartz rate monitor (using the graphite density for reference), is about 100 nm. However, since the real density of the films can be quite different, absolute measurements of the number of carbon atoms deposited are performed using the Rutherford backscattering spectrometry (RBS) technique for 2-MeV α particles. The electronic structure of the synthetized materials is studied by FTIR (Fourier-transform-infrared-absorption spectroscopy),[6] RS (Raman scattering), EELS (electron-energy-loss spectroscopy),[6] XANES (x-ray-absorption near-edge spectroscopy)[6] and AES (Auger-electron spectroscopy).[6] Structural information is obtained by AFM (atomic force microscopy),[6] SEM (scanning electron microscopy)[6] and transmission electron diffraction.[6] One has to mention that AES and XANES revealed no bonded oxygen in the films. The estimated concentration of bonded hydrogen in our films measured by the nuclear reaction ^1H (^{15}N, $\alpha\gamma$) ^{12}C is about 4–5%. Such a concentration is usually found in common amorphous semiconductors such as poorly hydrogenated silicon or amorphous carbon. For Raman analysis, our carbon samples were investigated in the backscattering configuration (Dilor XY with a charge coupled device camera detector) at room temperature. The beam of an argon-ion laser operating at a wavelength of 514.5 nm was focused down to a 100-μm^2 spot in a confocal microscope. However, the metastable samples

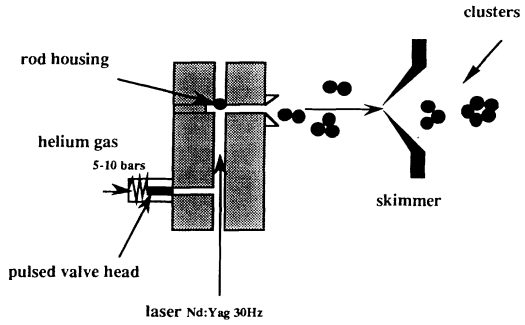

a schematic view of the cluster source

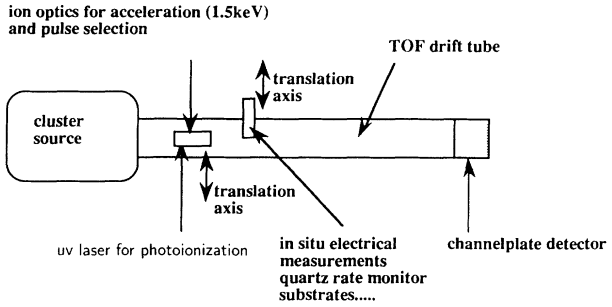

b schematic view of the deposition line

FIG. 1. Cluster beam setup (a) and time-of-flight and deposition chamber setup (b).

are generally very sensitive to the annealing effect under laser irradiation. Consequently, to avoid the graphitization process, the exposure time and laser power have been optimized (irradiation time less then 10 min laser power less than 10 mW). A schematic view of the cluster beam setup is shown in Fig. 1.

III. FREE CLUSTERS PROPERTIES

An abundance mass spectrum is given in Fig. 2. The greatest intensities of some peaks (corresponding to magic numbers) are usually due to the presence of clusters of enhanced stability. The ion cluster sequence ($n=11$, 15, and 19, with a periodicity of $\Delta n=4$), already observed by several authors[7,8] is easily understood by invoking aromaticity and the completion of electronic shells. This occurs for $(4n+2)$ π electrons in neutral clusters ($n=10$, 14, and 18) and $(4n+3)\pi$ electrons in cations. Such considerations on the aromatic structure favor the sp^2 hybridization.

Beyond $n=32$ the even/odd alternance (C_{2n}/Cn_{2n+1}) is characteristic of the existence of the three-dimensional structures known as fullerenes.[9] The fullerenes correspond to graphite honeycomb sheets bent into closed cages by the replacement of 12 hexagons by pentagon rings. Using the empirical isolated pentagon rule

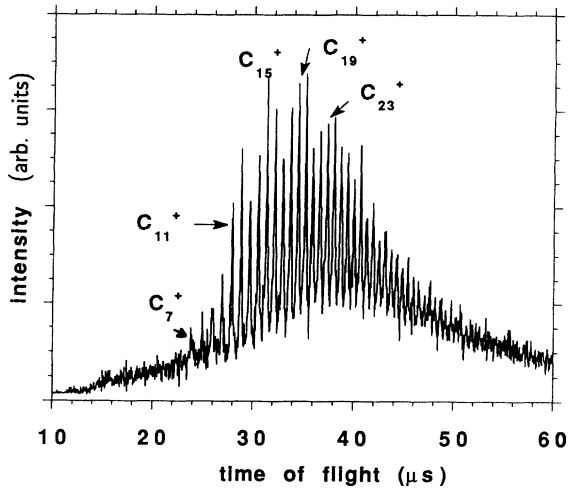

FIG. 2. Abundance mass spectrum of ion carbon clusters. Magic numbers are labeled in the figure.

(IPR),[10,11] the first stable fullerene is C_{60}. However, we admit that the fullerene structure is favored beyond C_{32}. Some theoritical calculations predict the possible existence of spheroidal cages in the range $n=20-32$ (12–13). The first hypothetical fullerene C_{20} is a dodecahedron (I_h symmetry) having an open shell structure. Each atom is threefold bonded with atomic orbitals orientations (108° neglecting Jahn-Teller distortion) close to those in the blende structure (109°28′). The corresponding σ-η interorbital angle ($\theta_{\sigma\pi}$) is about 110°50′ ($\theta_{\sigma\pi}=90°$ in graphite and $\theta_{\sigma\pi}$ 109°28′ in diamond).[14] This unstable molecule can be stabilized, for example, by atomic hydrogen trapping ($C_{20}H_{20}$) acquiring pure sp^3 hybridization. The same consideration on the other fullerenes in the range $n=20-30$ show that their hybridization is also close to sp^3.[14] However, in this range of sizes, closed cages are much less stable that open curve graphitic sheets which minimize the number of adjacent pentagon rings.[15] Therefore, the relative population of fullerenes is governed by cluster growth kinetics. In our cluster source, the high sursaturation ratio involves a great number of cluster-helium-gas collisions, allowing consequently a low vibrational temperature. Finally, we conclude that some unstable particles such as small fullerenes may be produced in our experimental device. Their production is not completely evident with regard to the mass spectra only, but we think that the specific nature and properties of our films described in Sec. IV agree with the hypothesis.

IV. FILM GROWTH

Neutral clusters are deposited on different substrates at room temperature with their kinetic energy (around 10 eV). In this case, the energy per atom is lower than the cohesive energy of a cluster and, consequently, the film is formed by the random stacking of these particles without any fragmentation process. In previous papers, we showed that the hybridization of carbon in the films was controlled by the mean hybridization of the incident free clusters. In the present experiments we thus expect a hy-

bridization close to sp^3 in the films obtained by deposition of clusters, the mass distribution of which is centered around C_{20} (see Sec. III). This electronic structure is confirmed by several complementary experiments.[6] In particular, a weak contribution of π electrons is observed in the experimental density of states of conduction and valence bands studied by EELS and XANES, respectively.[6]

For reasons of convenience, we will call the samples synthetized by deposition of a size distribution centered around C_{20} "C_{20} films."

The diffraction patterns of the C_{20} films exhibit two diffuse rings in agreement with a disordered or amorphous state. The position of these diffuse rings (halos) can be related to the atomic planes $d_{111}=0.206$ nm and $d_{220}=0.126$ nm in the fcc-diamond (blende structure).[16] We can thus expect that the first-neighbor distances in our films are close to the diamond value (0.154 nm). The granular structure of our films, as observed by SEM and AFM, should be compared to a "nanosponge." Consequently, a film density of 0.8 ± 0.2 g cm^{-3}, much lower than the diamond density (3.5 g cm^{-3}) and even any pure carbon phase, has been measured.

V. FIRST-ORDER RAMAN ANALYSIS

A. Background theory

It is interesting to compare the disordered structure of the C_{20} films with the disordered structure of the common covalent semiconductors such as amorphous silicon. For this purpose, we use the selection rule breakdown concept developed by Shuker and Gammon[17] to understand our Raman-scattering measurements. These authors showed that the Raman intensity of light scattered by a disordered materials, at the frequency $\omega/2\pi$, can be written as

$$I_{\alpha\beta,\gamma\delta}(\omega)=\sum_{\text{all the bands b}} C_b^{\alpha\beta,\gamma\delta}\left[\frac{1}{\omega}\right][1+n(\omega,T)g_b^a(\omega)]\ . \tag{1}$$

$[n(\omega,T)+1]$ is the Böse factor for Stokes scattering, T the sample temperature, $g_b^a(\omega)$ the vibrational density of states (DOS) in the b band and $C_b^{\alpha\beta,\gamma\delta}$ the optical coupling tensor which describes the coupling of phonons and photons via the electronic polarizability tensor of the material. Shuker and Gammon assign frequency-independent coupling constants for all bands leading to an approximate expression given by

$$I(\omega)=\sum_{\text{all the bands b}} C_b\left[\frac{1}{\omega}\right][1+n(\omega,T)g_b^a(\omega)]\ . \tag{2}$$

In covalent semiconductors, where the bonds between atoms are quite similar to those in the crystalline phase, with nearly the same coordination number, bond lengths, and bond angles, the electronic structure of an amorphous semiconductor is slightly disturbed compared to the corresponding crystal.[18,19] In a simple approach, the first-order Raman scattering of amorphous covalent materials corresponds to the broadened phonons DOS.[20,21] This simple model is verified in the case of common semiconductors such as amorphous silicon.[22] In addition, a Raman peak shift, which can sometimes be observed, is usually attributed to a change of the force-constant values and the broadening of the lines is caused by structural disorder.

To date, all tetrahedrally bonded amorphous semiconductors have been evidenced in this manner, with the exception of carbon.

B. Results

The reduced Raman scattering intensity measured with our C_{20} films is given in Fig. 3. We can see that the experimental curve and the calculated phonons DOS of fcc diamond (inset) obtained by Pavone *et al.*[23] exhibit very similar features. However, some differences are clearly observed.

(i) Contrary to common group-IV semiconductors, we observe a DOS without any broadened bands as suggested above, except maybe for the TO branch.

(ii) The labeled TA band is not as flat as in diamond, but seems close to other materials such as silicon, germanium, grey tin, and GaAs.[24]

(iii) The whole spectrum is shifted by 130 cm^{-1} toward the low-energy values.

These observations are not consistent with the usual continuous random network model, which considers a density value close to the crystal one. Thus, to understand the particularities of our Raman spectrum, we introduce a topological network by considering the following hypothesis.

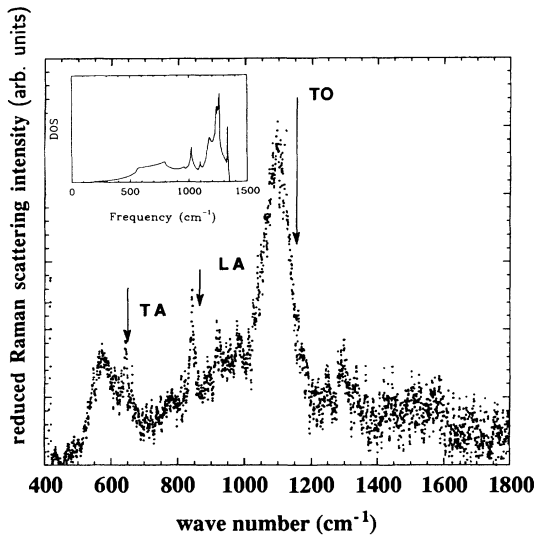

FIG. 3. Reduced first-order Raman-scattering spectrum obtained with a confocal micro-Raman spectrometer Dilor *XY*. $I_R(\omega)$ has the form $I_R(\omega)=I(\omega)/[\omega([n(\omega)+1])]$, where $I(\omega)$ is the experimental Raman scattering, and $n(\omega)$ is the Böse factor. The thickness of the C_{20} film was about 100 nm. The photon excitation wavelength was 5145 Å. To avoid the graphitization process, the power was limited to 10 mW, and the exposure time was about 5 min. The spectrum in the inset is the calculated phonon density of states for carbon in the fcc diamond phase (Ref. 23).

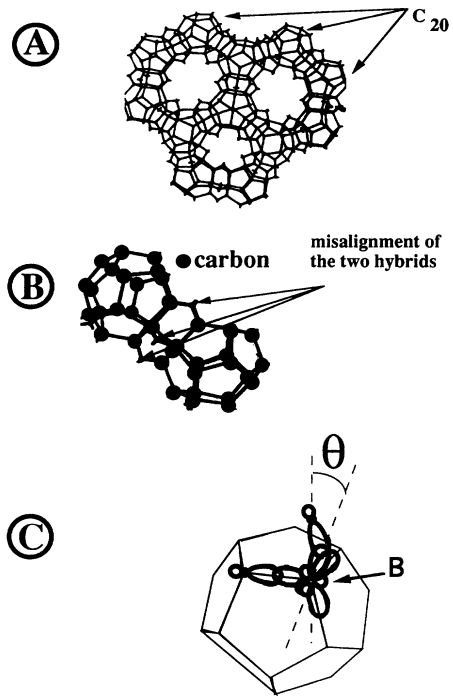

FIG. 4. Random compact cluster stacking (RCCS) (a), detail of the misalignment of the two hybrids between two clusters (b), and definition of the θ angle (c).

(i) Pure C_{20} cluster deposition, without fragmentation on the substrate, allows the geometry of C_{20} cluster to be conserved (bond lengths and angles).

(ii) Clusters nucleate on the substrate to minimize the dangling-bond number.

(iii) Despite the presence of destabilizing π bonds on pentagons, force constants of diamond are introduced in our calculations. This point will be discussed elsewhere.

Figure 4(a) shows a C_{20} network formed by giant hexagons and pentagons. These caps appear to be precursors of an hypothetic $(C_{20})_{60}$ fullerene, where we put a C_{20} cluster in the place of one atom in the normal C_{20} fullerene. Probably such giant clusters do not grow in our film because we deposit a rather broad cluster size distribution. However, we can imagine that a random stacking of some pieces of this structure contribute to the film growth. The existence of empty areas is evidenced by this model and is consistent with density measurements. One obtains the same bond lengths between adjacent clusters as in intracluster $d_{C\text{-}C}$ bond lengths. Furthermore, two clusters are bonded by their pentagon face involving π bonds [see Fig. 3(b)]. The growth without any dangling bond cannot be achieved at long-range order because the translational symmetry is forbidden by C_{20} I_h symmetry.

1. Tight-binding model

From the previous model, we can build a simple tight-binding model with a LCAO (linear combination of atomic orbitals) Hamiltonian. The hypothesis are the following.

(i) The bond-orbital model and the LCAO Hamiltonian are assumed.

(ii) The valence force field and the classical elastic model approximations are valid.

(iii) The interaction parameters in the cluster are identical to the diamond parameters.

(iv) Despite the nontranslational symmetry of the network, we apply the Bloch theorem assuming a local quasiperiodicity.

One has to remember that in diamond, the hybrid covalent energy V_h is defined as the matrix element between hybrids pointed at each other from two neighboring atoms. For this misaligned hybrids, the hybrid covalent energy is obtained assuming the hybrid decomposition from σ and π states. If we now examine the detail of two linked C_{20} [Fig. 4(b)], we can see that each atom on a pentagon edge is bonded in three directions by conventional hybrids, and in the fourth direction by one misaligned bond. θ is the corresponding angle of misalignment. To keep the tetrahedrally coordonated structure, the atom labeled B must rotate by θ angle ($\theta \approx 35°$). Using the bond orbital approximation and the valence force field model, one obtains the optical modes (corresponding to the Raman frequency in the crystal) as a function of the hybrid covalent energy.[25] We can write the ratio between the hybrid covalent energy defined previously in our system and the hybrid covalent energy in a pure sp^3 basis. The corresponding transverse optical mode shift is[25]

$$\frac{\Delta\omega_{\mathrm{TO}}}{\omega_{\mathrm{TO}}} = \left[\frac{\left[-V_{ss} + \frac{\sqrt{3}}{2} V_{sp\sigma}(\cos\theta + 3) + \frac{3}{4} V_{pp\sigma}(\cos^2\theta + 3) - \frac{3}{4}\sin^2\theta V_{pp\pi} \right]}{(-V_{ss} + 2\sqrt{3}V_{sp\sigma} + 3V_{pp\sigma})} \right]^{1/2} - 1 . \tag{3}$$

This formalism can be extended to all phonon branches. Qualitatively, we find a decrease (2%) of the constant force which leads to a redshift of the reduced Raman spectrum. However, the experimental shift is much higher (about 10%). This can be understand having in mind hypothesis (ii). In fact, the C_{20} cluster interatomic force constants are lower than the diamond ones, because the nonpaired π electrons located on the C_{20} cluster destabilize the bond. Furthermore, the previous model does not take into account the experimental size dispersion. We thus observe a large decrease of the TO mode frequency compared to diamond. The formalism developed for the hybrid covalent energy calculation can be extended to the other LCAO Hamiltonian ele-

ments. The resulting band structures for diamond and our expected model are shown in Fig. 4. The energy separation between the valence-band maximum at Γ and the conduction-band minimum is overestimated because the LCAO tight-binding model is not accurate enough. We observe a strong decrease of the gap (factor 2) at the threefold-degenerated Γ point.

2. *Redshift and intense TA branch*

In the Raman spectrum of amorphous silicon, the small shift of the TO band compared to the crystal is not due to a weakening of the force constants but to a broadening effect. One of the reasons is that the Raman frequency allowed in the crystal is higher than the phonon DOS maximum. In our case, the redshift cannot be explained with this argument. In addition, for common semiconductors, it is well known that a small shift can occur either by the film growth mode,[26,27] thickness effect,[28] or hydrogen concentration.[29] However, to our knowledge a shift value as high as 130 cm^{-1} has never been observed in common semiconductors. In our case, as mentioned above, the tight-binding model suggests a weakening of the force constant in the expected film structure which can explain the redshift.

It is well known that the TA-mode density is sensitive to the long-range forces. Except in diamond, the TA-phonon branches are very flat away from the Brillouin-zone center.[24] Consequently, for all materials with a diamond structure, the DOS exhibits an enhancement of the TA branches. The displacement of an atom tends to rotate the neighboring tetrahedra of hybrids[25] inducing a rotation of these neighbors, and so at long distances a propagating pseudowave disturbs atoms. Weber[30] has shown that this behavior can be understood from interactions involving the bond charges. In diamond, the ion bond charge coupling is much stronger than in the other materials; consequently the bond-bond interaction increases to a lesser extent. Sokel and Harrison[31] proposed a physical explanation of these long-range forces in terms of electronic structure. These authors have shown that the interaction energy contains a decay exponential term assigned to a screening length $[k_g^{-1}]$. The ratio of screening length to zone-boundary wavelength ($k_0=2\pi/a$) gives the long-range order of the interbond force constants. These authors have shown that the longest range forces come from the states close to the band gap,

$$k_g^2=(2(m_1+m_2)/\hbar^2)E_g \ , \tag{4}$$

where m_1 and m_2 are the valence and conduction-band electron effective masses, and E_g is the energy gap.

The great gap for diamond involves a strong screening length, as the mentioned by Weber.[33] The data of Sokel and Harrison for k_0/k_g are given in Table I can be compared with our C_{20}-film data.

The strong decrease of the gap in the C_{20} film agrees with an enhancement of the long-range forces. Therefore, our spectrum exhibits an intense TA-phonon branch far away from the Brillouin-zone center. Finally, the behavior of the TA-phonon branch and the energy shift of the Raman band have the same origin. Such results

TABLE I. Extrapolated value from the tight-binding model.

Element	k_0/k_g	$k_0=2\pi/a$ ($Å^{-1}$)
C	1.7	1.764
Si	3.1	1.159
Ge	4.8	1.111
our sample	2.4	1.25

can be compared with Raman shifts in hydrogenated microcrystalline silicon observed by of Iqbal and Veprek.[32] These authors found that shifts to lower frequencies with decreasing crystallite size of the crystalline components of the spectra have been correlated with the lattice expansion and the finite dimensions of the crystallites in these films. Other surface effects were observed in thin slabs of silicon by Kanellis, Morhange, and Balkenski.[28] In our case, all the atoms are located on the cluster surface, so we believe that our films exhibit a maximum surface effect which explains the shift amplitude. However, the lattice expansion (or contraction) in the C_{20}-films is not observed because the electron-diffraction pattern data are not accurate enough.

3. *Line broadening effect*

As mentioned in Sec. V B the broadening effect is explained by structural disorder.[33] Except for TO branches, the correlation between the calculated diamond phonon DOS and the reduced Raman spectrum is remarkable. This one suggests a very low disorder at short-

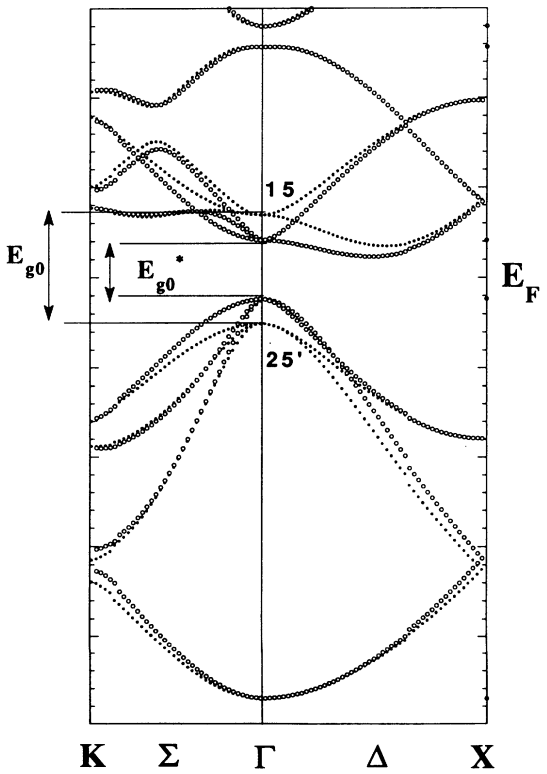

FIG. 5. Band structure of diamond (●) and C_{20} (○). E_{g0} and E_{g0*}, respectively, are the gap of the diamond and the C_{20} film.

and medium-range orders contrary to classical amorphous networks such as a-Si or a-Ge. This assumption is in good agreement with the fine structure observed by XANES with our samples compared to XANES spectra of amorphous semiconductors which generally do not exhibit fine structure because of the perturbations of electronic structure by disorder. In our model, the distance is the same for all first-neighbor atoms. At last, the slight broadening of the TO branch compared to the calculated phonon DOS may be explained by the strong perturbation of the electronic band diagram along the ΓX axis (Fig. 5).

C. Annealing effect

The metastability of the sample is clearly observed during intense laser irradiation. An increase of the laser power up to 100 mW leads to the sample partial annealing. A typical Raman-scattering spectrum obtained in this case is given in Fig. 6. The spectrum shows three broad bands. Two bands labeled D and G (D for the disorder-induced mode, G for the Raman-allowed graphite mode) are clearly observed as in common diamondlike films.[1] The next band labeled C, deduced from a decomposition of the spectrum into individual Gaussian components, is observed around 1150 cm^{-1}. This one is assigned by many authors to pure diamond nanocrystallites features.[34,35] During laser irradiation, the C_{20} sample undergoes a phase transition (the so-called "graphitization" process). This is in agreement with EELS measurements showing the π-plasmon peak appearance (6.4 eV), characteristic of graphite.

We apply the Shuker and Gammon formalism to described the phase corresponding to small graphitic islands embedded in an sp^3-hybridized matrix. If the number of sp^2 clusters is low enough, the Raman-scattering intensity is calculated using the first-order perturbation model:

$$I(\omega)=A\sum_{\text{all the bands b}} C_{b(\text{graphite})}(1/\omega)[1+n(\omega,T)]g^{a}_{b(\text{graphite})} +B\sum_{\text{all the bands b}} C_{b(\text{diamond})}(1/\omega) \times[1+n(\omega,T)]g^{a}_{b(\text{diamond})} . \quad (5)$$

A and B are two numerical factors including the relative population of small sp^2 islands in the matrix.

In Fig. 6(c), we show the calculated graphite phonon DOS given by Al-Jishi and Dresselhaus[36] broadened by a factor of about 40 cm^{-1}. Using Eq. (5), we can fit the Raman spectrum of our samples after annealing [Fig. 6(a)] by adding the spectrum before annealing [Fig. 6(b)] an the theoretical spectrum corresponding to the graphite phonon DOS mentioned above [Fig. 6(c)]. The relative intensity of both components is obtained by the A/B ratio adjustment. However, taking into account the different Raman efficiencies of diamond and graphite, no accurate quantitative results for the sp^2/sp^3 ratio can be deduced. After a strong annealing, the C band disappears, and we observe an increase of the G/D ratio.

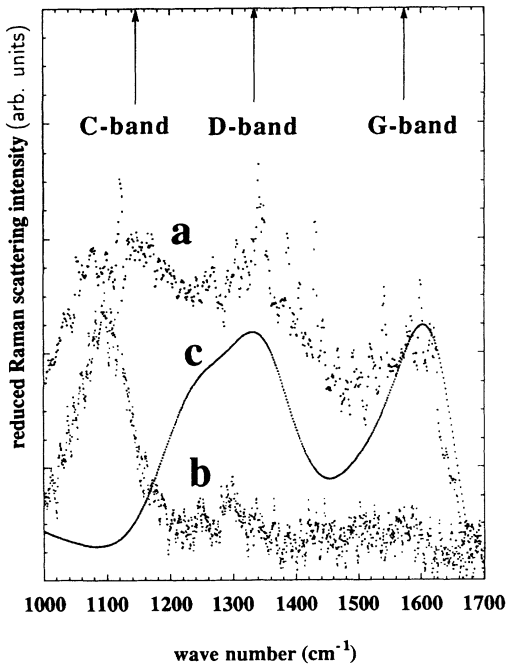

FIG. 6. Reduced Raman scattering of the sample after annealing (a), before annealing (b), and the graphite phonon DOS (c) deduced from the theoretical dispersion curves given by Al-Jishi and Dresselhaus (Ref. 36). The C, D- and G-band positions are shown by the arrows.

VI. CONCLUSION

The specific structures and properties of our films obtained by low-energy neutral cluster beam depositions are clearly deduced from the Raman spectra. Conductivity measurements, optical and infrared spectroscopies, and secondary electron emission spectroscopy corroborate the results. The films formed by cluster deposition keep the memory of the free cluster electronic structure. This is observed with the C_{20} films but also with other deposited mean cluster sizes (C_{60} and C_{900}).[37] In each case, the hybridization observed in the films can be correlated to the hybridization of the mean free cluster size. To keep the free cluster memory, the structure of the film must be different from the classical random network, as proposed by Polk. The film appears as nanocrystallite stacking called random compact cluster stacking (RCCS). Thermodynamically, this network is energetically unfavorable, which explains the metastability of the film. Indeed, in common semiconductors, the bond length and bond angle fluctuations are weak and randomly distributed among the atoms. In our system, the fluctuations are strongly localized between the clusters, which is energetically highly unfavorable.

Furthermore, since the diamond phonon density of states has never been observed to our knowledge in the first-order reduced Raman spectra of amorphous carbon films, it is important to note that we may have produced small fullerenes in our experimental device thereby explaining the specific nanostructure of our films at the ori-

gin of our Raman spectroscopy observations. This is surprising because small fullernes such as C_{20} are highly unstable, as predicted by theory. We attribute our results to the specific cluster growth and film growth conditions; the nonequilibrium state, low vibrational temperature attained during the vacuum expansion and low transit time (about 100 μs) between the cluster formation and its deposition on the substrate where it can be stablized by nucleation. Therefore, the properties of our films can be related to strong surface effects if we remember that all the atoms in C_{20} or similar clusters are surface atoms. The surface/bulk ratio is not a function of the film thickness in the RCCS model, expect that the properties of our films are preserved in thicker films.

Finally, the RCCS technique using low-energy neutral cluster beam deposition seems to be a promising technique for synthesis of new materials. In the particular case of covalent materials, after the interesting results with carbon, complementary studies with silicon would be helpful.

[1] *Diamond and Diamondlike Films and Coatings,* Vol. 266 of *NATO Advanced Study Institute, Series B: Physics,* edited by R. E. Clausing *et al.* (Plenum, New York, 1991), pp. 481–498.

[2] P. Melinon, G. Fuchs, B. Cabaud, A. Hoareau, P. Jensen, V. Paillard, and M. Treilleux, J. Phys. (France) I, **3**, 1585 (1993)

[3] R. E. Smalley, Laser Chem. **167**, 2 (1983).

[4] J. R. Heath, Y. Liu, Q. L. Zhang, R. F. Curl, F. K. Tittel, and R. E. Smalley, J. Chem. Phys. **83**, 5520 (1985).

[5] W. A. de Heer and P. Milani, Z. Phys. D **20**, 437 (1991).

[6] V. Paillard, Ph.D thesis, University of Lyon, 1993.

[7] E. A. Rohlfing, D. M. Cox, and A. Kaldor, J. Chem. Phys. **81**, 3322 (1984).

[8] L. A. Bloomfield, M. E. Geusic, R. R. Freeman, and W. L. Brown, Chem. Phys. Lett. **318**, 162 (1985).

[9] H. W. Kroto, J. R. Heath, S. C. O'Brien, R. F. Curl, and R. E. Smalley, Nature **318**, 162 (1985).

[10] T. G. Schmalz, W. A. Seitz, D. J. Klein, and G. E. Hite, Chem. Phys. Lett. **130**, 203 (1986).

[11] Q. Zhang, S. C. O'Brien, J. R. Heath, Y. Liu, R. F. Curl, H. W. Kroto, and R. E. Smalley, J. Phys. Chem. **90**, 525 (1986).

[12] B. L. Zhang, C. Z. Zhang, K. M. Ho, C. H. Xu, and C. T. Chan, Phys. Rev. B **46**, 7333 (1992).

[13] D. Bakowies and W. Thiel, J. Am. Chem. Soc. **113**, 3704 (1991).

[14] R. C. Haddon, J. Am. Chem. Soc. **108**, 2837 (1986).

[15] J. R. Heath, in *Fullerenes: Synthesis, Properties and Chemistry of Large Carbon Clusters,* ACS Symposium No. 181, edited by G. S. Hammond and V. J. Kuck (Am. Chem. Soc., Washington, D.C., 1992), pp. 1–23.

[16] *Joint Committee on Powder Diffraction Standards,* Natl. Bur. Stand. (U.S.) Circ. No. 539 (U.S. GPO, Washington, D.C., 1953), Vol. 2, p. 5.

[17] R. Shuker and R. W. Gammon, Phys. Rev. Lett. **25**, 222 (1970).

[18] D. E. Polk, J. Non-Cryst. Solids **5**, 365 (1971).

[19] D. Weare and M. F. Thorpe, Phys. Rev. B **4**, 2508 (1971).

[20] *Topics in Applied Physics: Light Scattering in Solids,* edited by M. Cardona (Springer-Verlag, Berlin 1975), pp. 205–227.

[21] J. E. Smith, Jr., M. H. Brodsky, B. L. Crowder, and M. I. Nathau, in *Proceedings of the Second International Conference on Light Scattering in Solids,* edited by M. Balkanski (Flammarion, Paris, 1971), pp. 330–334.

[22] C. C. Tsai and R. J. Nemanich, J. Non-Cryst. Solids **35-36**, 1203 (1980).

[23] P. Pavone, K. Karch, O. Schütt, W. Windl, D. Strauch, P. Giannozi, and S. Baroni, Phys Rev. B **48**, 3156 (1993).

[24] R. Tubino, L. Piseri, and G. Zerbi, J. Chem. Phys. **56**, 1022 (1971).

[25] W. A. Harrison, *Electronic Structure and the Properties of Solids (The Physics of the Chemical Bond)* (Freeman, San Francisco 1980), pp. 180–219.

[26] J. S. Lannin, L. J. Pilione, S. T. Kshirsagar, R. Messier, and R. C. Ross, Phys. Rev. B **26**, 3506 (1982).

[27] N. Maley, L. J. Pilione, S. T. Kshirsagar, and J. S. Lannin, Physica (Amsterdam) **117B/118B**, 880 (1983).

[28] G. Kanellis, J. F. Morhange, and M. Balkanski, Phys. Rev. B **21**, 1543 (1980).

[29] J. S. Lannin, in *Semiconductors and Semimetals,* edited by J. I. Pankove (Academic, New York, 1984), Vol. 21, Part B, pp. 159–191.

[30] W. Weber, Phys. Rev. Lett. **33**, 371 (1974).

[31] R. Sokel and W. A. Harrisson, Phys. Rev. Lett. **36**, 61 (1976).

[32] Z. Iqbal and S. Veprek, J. Phys. C **15**, 377 (1982).

[33] J. S. Lannin, J. Non-Cryst. Solids **97-98**, 39 (1987).

[34] I. Watanabe and K. Sugata, Jpn. J. Appl. Phys. **27**, 1808 (1988).

[35] R. J. Nemanich, J. T. Glass, G. Lucovsky, and R. E. Shroder, J. Vac. Sci. Technol. A **6**, 1783 (1988).

[36] R. Al-Jishi and G. Dresselhaus, Phys. Rev. B **26**, 4514 (1982).

[37] V. Paillard, P. Mélinon, V. Dupuis, J. P. Perez, A. Perez, and B. Champagnon, Phys. Rev. Lett. **71**, 4170 (1993).

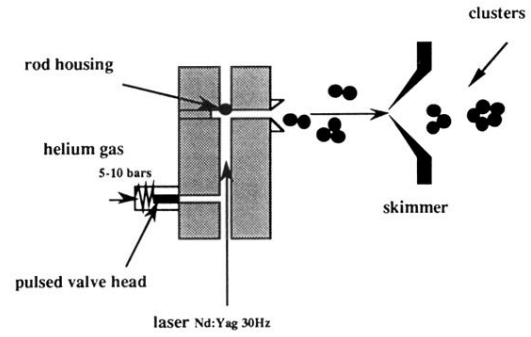

a schematic view of the cluster source

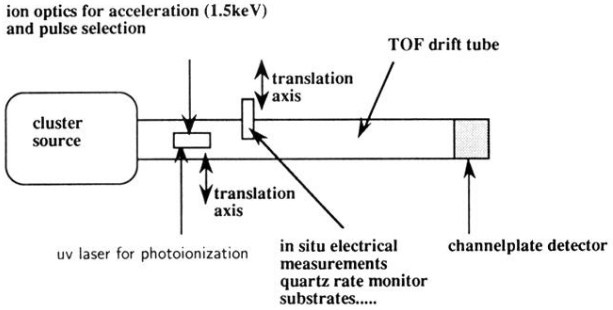

b schematic view of the deposition line

FIG. 1. Cluster beam setup (a) and time-of-flight and deposition chamber setup (b).